Tree crown detection in high resolution optical and LiDAR images of tropical forest

Jia Zhou, Christophe Proisy, Xavier Descombes, Ihssen Hedhli, Nicolas Barbier, Josiane Zerubia, Jean-Philippe Gastellu-Etchegorry, Pierre Couteron

Tree crown detection in high resolution optical and LiDAR images of tropical forest

Jia Zhou[ac], Christophe Proisy[b], Xavier Descombes[c], Ihssen Hedhli[c], Nicolas Barbier[b], Josiane Zerubia[c], J. P. Gastellu-Etchegorry[d] and Pierre Couteron[b]

[a]Université Montpellier II, UMR AMAP, Montpellier, France;
[b]IRD, UMR AMAP, Montpellier, France;
[c]Ariana Research Group, INRIA/I3S, Sophia-Antipolis, France;
[d]Université Paul Sabatier, UMR CESBIO, Toulouse, France

ABSTRACT

Tropical forests are complex ecosystems where the potential of remote sensing has not yet been fully realized. The increasing availability of satellite metric imagery along with canopy altimetry from airborne LiDAR open new prospects to detect individual trees.

For this objective, we optimized, calibrated and applied a model based on marked point processes to detect trees in high biomass mangroves of French Guiana by considering a set of 1m pixel images including 1) panchromatic images from the IKONOS sensor 2) LiDAR-derived canopy 2D altimetry and 3) reflectance panchromatic images simulated by the DART-model. The relevance of detection is then discussed considering: (i) the agreement in space of detected crown centers locations with known true locations for the DART images and also the detection agreement for each pair of IKONOS and LiDAR images, and (ii) the comparison between the frequency distributions of the diameters of the detected crowns and of the tree trunks measured in the field. Both distributions are expected to be related due to the allometry relationships between trunk and crown. Results are encouraging provided that crown sizes sufficiently large compared to 1m pixels.

Keywords: Tropical forest, tree detection, mangrove, marked point process, IKONOS, LiDAR, DART

1. INTRODUCTION

Monitoring tropical forest structure is a very difficult but essential objective for quantifying levels of degradation and carbon stocks in such complex and dense vegetation ecosystems. For this, the potential of remote sensing is to be examined in relation to the regular improvement and diversification of sensors. This is particularly true for very high resolution (VHR) images with metric and sub-metric pixels as provided by IKONOS, QuickBird, Geoeye, TerraSAR-X satellites and the forthcoming "ORFEO" dual Earth observation system with radar (ASI "Cosmo-Skymed") and optic (CNES "Pleiades-HR") components. Also the LiDAR-derived canopy height images are VHR data which can be useful references to assess the relevance of analyses applied to optic data.

Submitting VHR imagery to texture analysis yielded relevant information on the upper part of the forest volume, i.e. the forest canopy [1,2], which proved correlated with important forest attributes as above-ground biomass (AGB). In comparison, both optical and radar derived intensities are unable to represent the whole range of structural variation observable in tropical forest, because signal is saturated at the midlevel of leaf area index and total AGB (e.g. [3] and [4]), while for texture indices saturation was not observed up to AGB values of more than 500 tons of dry matter per hectare ($t\ DM\ ha^{-1}$).

Further author information:
J. Zhou, C. Proisy, N. Barbier and P. Couteron: Boulevard de la Lironde, TA A51-PS2, 34398 Montpellier cedex 5, France
E-mail: jia.zhou@cirad.fr, christophe.proisy@ird.fr, nbarbier@ulb.ac.be, pierre.couteron@ird.fr
X. Descombes, I. Hedhli and J. Zerubia: 2004, route des Lucioles, BP 93, 06902, Sophia-Antipolis cedex, France
E-mail: xavier.descombes@sophia.inria.fr, ihsen.hedhli@sophia.inria.fr, josiane.zerubia@sophia.inria.fr
J. P. Gastellu-Etchegorry: 18 Av. Ed. Belin, 31401 Toulouse, France
E-mail: Jean-Philippe.Gastellu@cesbio.cnes.fr

In this paper we explore the potential of VHR data in another direction that is characterizing individual canopy trees in terms of locations and crown sizes. For that, we used a stochastic geometry approach based on marked point processes (MPP) which has been successfully tested for the detection of flamingos on aerial photographs of a colony [5]. We apply the MPP approach to optic IKONOS and air-borne LiDAR VHR images acquired over mangrove forests and also test the method on simulated canopy images using the DART radiative transfer model [6].

2. DATA

2.1 Forest data

Forest areas for field sampling were selected in the region of Sinnamary, French Guiana with the aim of capturing the largest range of mangrove dynamic stages. Field measurements were carried out from 2002 to 2005 [1] and yielded AGB values ranging from 80 to 410$t\ DM\ ha^{-1}$. For this work, we selected 3 mangrove plots showing a contrasted gradient in their canopy structure as shown in Figure 1. This gradient included three close canopy stages: (i) young trees with small crowns (young stage: YS), (ii) adult trees with large crowns (mature stage: MS1 and MS2) and (iii) open canopy where adult trees with large crowns were sparsely distributed (decaying stage: DS).

2.2 Metric resolution images

This study is based on the analysis of both real-world and simulated images all sharing the same spatial resolution (1m pixels). One panchromatic IKONOS image acquired in 2003 and a LiDAR-derived canopy altimetry image obtained in 2004 were selected because of their overlapping over the area of study (Figure 1). The LiDAR system includes a portable Riegl laser rangefinder (LMS6Q140i-60) mounted onboard a helicopter flying at a speed of $30ms^{-1}$ about $150m$ above the ground. Further information on the Lidar data acquired over the area of study is available in [7]. For comparison with the IKONOS data, we sampled the LiDAR-derived altimetry image using a 1m pixel.

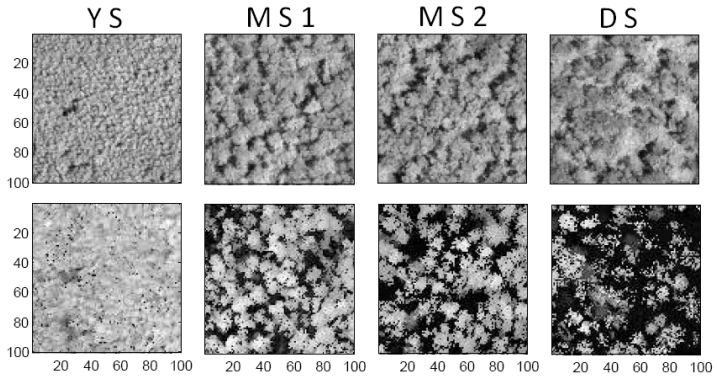

Figure 1. From left to right, plots of young, mature and decaying stages of mangrove imaged by IKONOS (top) and by LiDAR altimetry images (bottom).

To test and calibrate the MPP object detection process we used simulated forest canopy scenes, which were produced by the DART (Discrete Anisotropic Radiative Transfer) model [8][6]. The forest structures were generated to express a simple gradient of closeness/openness (Figure 2, on the left side). They include: a close canopy consisting of uniformly distributed trees with both identical height and crown diameters equal to 10 meters (Figure 2 #1), an opened canopy in which 20% of the trees generated in the previous template are removed (Figure 2 #2), and a more realistic template (Figure 2 #3) derived from allometric theory providing a priori values for tree size distributions and relationships between tree dimensions [9]. DART simulations were performed using sun and viewing angles of the IKONOS image with a pixel size of 1 meter to produce $100 \times 100m$ images of reflectance.

3. METHODS

3.1 The Marked Point Process model

Any remote sensing image of forests can be viewed as a space where positions and geometric attributes of tree crowns are a particular realization of a marked point process noted $\mathbf{x}$ (see [10,11] for more details). $\mathbf{x}$ is also a random variable whose realizations are random configurations of objects belonging to a state space $\chi = \mathcal{P} \times \mathcal{M}$, where $\mathcal{P}$ is the position space, and $\mathcal{M}$ the space of the marks (i.e. attributes of the objects).

The distribution of tree crowns within an image can then be represented by a marked point process of disks (which is only an approximate shape of tree crowns) and the associated space χ is then as following:

$$\chi = \mathcal{P} \times \mathcal{M} = [0, X_M] \times [0, Y_M] \times [r_m, r_M]$$

where X_M and Y_M are respectively the width and the length of the image I, r_m and r_M, the minimum and the maximum radius of the associated disk whose radius is considered as the mark.

The Gibbs density associated with such a marked point process of disks is defined with respect to the Poisson measure. Thus, the mathematical issue becomes an energy minimization including a regularization term also called the prior energy $U_p(\mathbf{x})$, which introduces some constraints on the objects and their interactions, and a data term $U_d(\mathbf{x})$, which shows how well the objects extracted fit to the image data.

In the case of tropical forest where tree crowns can overlap, the prior must consist in a soft penalization of overlapping disks in order to prevent over-detection of one tree by several overlapping disks (a pair of disks is considered as overlapping if their intersection is more than 10% of the smaller surface of the two disks): $U_p(\mathbf{x}) = \gamma\eta(\mathbf{x})$, where $\eta(\mathbf{x})$ is the number of pairs of intersecting disks in the configuration $\mathbf{x}$, and γ allows adjusting the prior energy importance compared to the data term. γ must be above 1 to penalize overlapping (we took $\gamma = 1.5$ and results were not influenced hy variations around this value).

The data term is also defined by a sum of local energies, $U_d(x_i)$, over all the objects x_i in the configuration. The local energy is obtained from the computation of a radiometric distance between pixels in the disk and pixels in the concentric annulus around the disk. A disk fits a tree in the image if and only if this radiometric distance significantly exceeds a certain threshold.

3.2 The Multiple Births and Deaths process

For optimizing the model, we consider a simulated annealing based on a multiple births and deaths process (MBD). This process has first been proposed in [12], whose algorithm is defined as follows:

1) **Initialize** the temperature parameter $T = 1$, the birth rate $\delta = (X_M \times Y_M)/r_M$ of the simulated annealing.

2) **Birth step:** for each pixel s in the image I, if there is no disk centered in s, we add an object in s, with a random radius between r_m and r_M, with probability $B(s)$, where $B(s)$ is proportional to δ and the data term in s (see [5] for details)

3) **Sorting step:** once the birth step is finished, we compute the data term $U_p(x_i)$ for each object x_i in the current configuration. Then, we sort them according to decreasing data energy.

4) **Death step:** for each object x_i taken in this order, we compute the death rate as follows:

$$d(x_i) = \frac{\delta \times a(x_i|\mathbf{x})}{1+\delta \times a(x_i|\mathbf{x})} \quad where: \quad a(x_i|\mathbf{x}) = \exp\left[\frac{\gamma \times \eta(x_i|\mathbf{x}) + U_d(x_i)}{T}\right]$$

$\eta(x_i|\mathbf{x})$ being the number of disks in $\mathbf{x}$ intersecting x_i.

This death rate is based on the energy variation that the object x_i brings to the total energy $U(\mathbf{x})$ of the model. If the addition of the object x_i increases the total energy, its death is highly probable.

5) **Convergence:** if the process did not converge, that is if the configuration has changed during the last iterations, then decrease T and δ and go back to step 2.

3.3 Assessing the detection performance of the MPP method

For simulated canopy images, the detection performance was evaluated by comparing detection results (crown centers and radii) with corresponding input parameters in DART. For real-word images we compared the results obtained from the analysis of the IKONOS and LiDAR data. For both comparisons, we implemented a likelihood test based on the Markov Random Field modeling to obtain indices of true and false detections.

In this test, we consider two sets of disks $X = x_i$ and $Y = y_i$, where Y is known as the reference, and X is the disk configuration obtained using the proposed approach. We match these two sets by considering the edges set $E = X \times Y$, coded as a binary variable such that $e_{ij} = 1$ if x_i is matched to y_j and 0 otherwise. An of the graphe optimization is executed based on the energy function associated with the Markov Random Field modeling. Then, if a disk in Y is matched with a disk in X, it is considered as a successful detection, otherwise it is a missed detection (omission error). If a disk in X is not matched with a disk in Y, it is considered as a false detection (commission error). Results on LiDAR images were used as reference (i.e. Y set) with respect to IKONOS.

Additionally, we used the field data,, that is tree trunk diameters at breast height (DBH) measurements in plots ($100m \times 100m$) , to check whether the frequency distribution of radii of the detected crowns may be consistent with the frequency distribution of trunks DBH. Indeed the allometric theory [9] predicts that DBH is linked to crown diameter (CD) by a power law as $CD \sim DBH^{\frac{2}{3}}$

4. RESULTS

In this section, we first present the detection results on DART images that helped deduce the parameters of the MPP algorithm to be used on the real-world images.

Figure 2 (on the right side) and Table 1 show the detections on the 3 DART images, with known values of crown radius used in the reference templates. For the first image, with a regular forest structure as a plantation, the detection demonstrates an exceptional performance, since almost all the trees were well detected. For the second image where vegetation cover has been decreased of about 20% compared to the first one, the detection became more difficult due to tree shadows. However, a majority of trees (98%) are detected with 6 (8.8%) false detections. As to the third image, in which the complexity of a real forest is mimicked, crown sizes in the template varied from 6m to 10m, and their shapes did not exactly correspond to disks (according to the allometric theory, tree crowns are modeled as ellipsoids). There were thus higher difficulties in detecting (Table 1). Only 21 out of 32 trees (66%) were detected in the image, with a high rate (25%) of false detection.

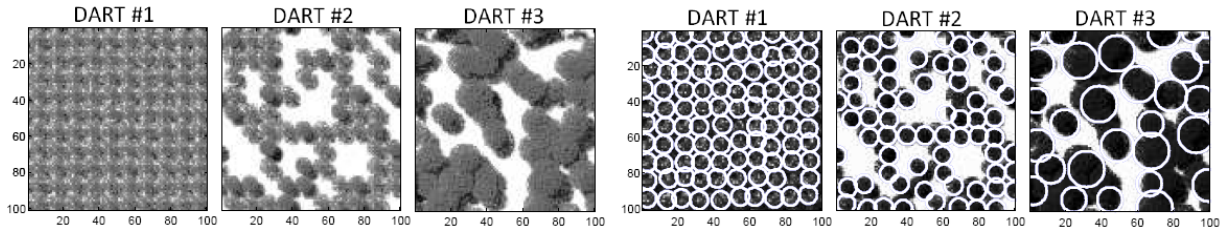

Figure 2. Left side: DART-simulated reflectance images for 3 forest templates. Right side: detections on these images.

Table 1. Detection performance using DART simulations.

	tree number in template	detected tree number	sucessful detections	false detections
DART #1	100	98	98 (98%)	0 (0%)
DART #2	63	68	62 (98%)	6 (8.8%)
DART #3	32	28	21 (66%)	7 (25%)

For the IKONOS and LiDAR images, the searched radius interval was defined between $r_{min} = 2m$ to $r_{max} = 10m$ according to field data. Then, the detection method was applied to every image separately, and the results are showed in Figure 3 and in Table 2.

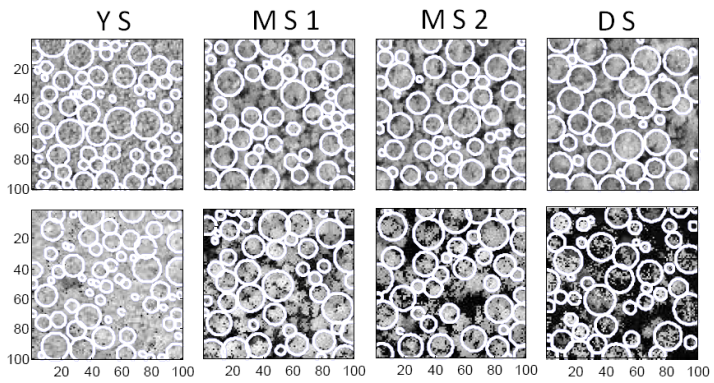

Figure 3. Detections on pairs of IKONOS (top) and LiDAR (bottom) images.

Table 2. Compared detection performance using IKONOS and LiDAR images.

	detected tree number		
	in LiDAR image	in IKONOS image	matching detections
plot YS	66	66	46
plot MS1	47	55	39
plot MS2	43	54	18
plot DS	49	42	35

Considering young stands, for which the crown diameters are of about 3m to 5m, as the plot YS in Figures 1 and 4, the spatial resolution of 1m was not sufficient to allow for an apparent space between crowns and the detection was not successful.

For each mature (MS1, MS2) and decaying (DS) field plots, trunk DBH histograms (field measures) presented two modes as did the histograms of crown diameters (detection on images). An example of these histograms is on the right side of Figure 4. The relationships between the values of the modes for DBH versus modes for crown diameters proved consistent with the order of magnitude predicted by the allometry theory, and the linear regression line fitted for the paired histogram modes was close to the predicted allometric relationship (after log-transformed values in Figure 4, on the left side).

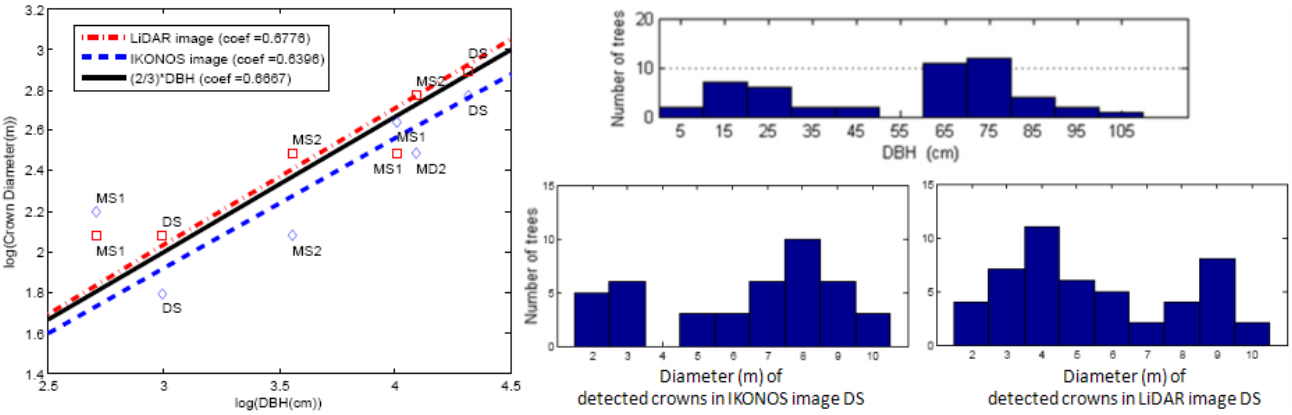

Figure 4. Comparing frequency distributions (histograms) for both trunk DBH measured in the field (top) and crown diameters detected on images (bottom). Right side: the histograms displayed two modes. Left side: scattered plots of the observed modes with fitted regression lines and mention of the curve (solid black) predicted by the allometric theory.

5. DISCUSSION

The results obtained in this study are rather encouraging for the application of the MPP crown detection method on VHR optical or LiDAR images from natural forests.

However, the sun angle plays an important role in image acquisition. Thanks to the DART model, we could analyze the different optical images obtained under variable acquisition parameters (as sun zenithal angle and sun to remote sensor angle). For the optical images taken over the French Guiana forest, the sun angle above the horizon varies often between 45° and 75° [2]. When this angle tends to 45°, tree shadows become more important in the images, and this perturb the detection (results not shown). In this study, we fixed the sun angle above the horizon at 70° for DART simulations, so the detection was not the most difficult. Nevertheless, the tree shadows disturbed the detection and determined many false detections, and future developments of the method should integrate the influence of acquisition parameters and derived shadowing.

ACKNOWLEDGMENTS

This research was supported by the joint INRA-INRIA AAP program (P00317) and by the Centre National d'Etudes Spatiales (CNES) for the preparation of the Dual optical system for metric resolution observations "Pleiades" mission.

REFERENCES

[1] Proisy, C., Couteron, P., and Fromard, F., "Predicting and mapping mangrove biomass from canopy grain analysis using fourier-based textural ordination of ikonos images," *Remote Sensing of Environment* **109(3)**, 379–392 (2007).

[2] Barbier, N., Couteron, P., Proisy, C., Malhi, Y., and Gastellu-Etchegorry, J. P., "The variation of apparent crown size and canopy heterogeneity across lowland amazonian forests," *Global Ecology Biogeography* **19(1)**, 72–84 (2010).

[3] Foody, G., Boyd, D., and Culter, M., "Predictive relations of tropical forest biomass from landsat tm data and their transferability between regions," *Remote Sensing of Environment* **85(4)**, 463–474 (2003).

[4] Mougin, E. and al., "Multifrequency and multipolarization radar backscattering from mangrove forests," *IEEE Transactions on Geoscience and Remote Sensing* **37(1)**, 94–102 (1999).

[5] Descamps, S., Descombes, X., Béchet, A., and Zerubia, J., "Flamingo detection using marked point processes for estimating the size of populations," *Traitement du Signal* **26** (2009).

[6] Gastellu-Etchegorry, J., Guillevicl, P., Zagolski, F., Demarez, V., Trichon, V., Deering, D., and Leroy, M., "Modeling brf and radiation regime of tropical and boreal forests: Brf," *Remote Sensing of Environment* **68**, 281–316 (1999).

[7] Proisy, C., Gratiot, N., Anthony, E. J., Gardel, A., Fromard, F., and Heuret, P., "Mud bank colonization by opportunistic mangroves: A case study from french guiana using lidar data," *continental Shelf Research* **29**, 632–641 (2009).

[8] Bruniquel-Pinel, V. and Gastellu-Etchegorry, J., "Sensitivity of texture of high resolution images of forest to biophysical and acquisition parameters," *Remote Sensing of Environment* **65(1)**, 61–85 (1998).

[9] West, G. B., Enquist, B. J., and Brown, J. H., "A general quantitative theory of forest structure and dynamics," *Proceedings of the National Academy of Sciences* **106(17)**, 7040–7045 (2009).

[10] Lieshout, M. N. M. V., "Markov point processes and their applications [hardcover]," *Imperial College Press* (2000).

[11] Perrin, G., Descombes, X., Zerubia, J., and Boureau, J., "Forest resource assessment using stochastic geometry," *International Precision Forestry Symposium* (2006).

[12] Descombes, X., Minlos, R., and Zhizhina, E., "Object extraction using a stochastic birth-and-death dynamics in continuum," *J Math Imaging Vis* **33**, 347–359 (2009).